Received: 18 June 2021 | Accepted: 12 August 2021

DOI: 10.1096/fj.202100930

THE FASEB JOURNAL

RESEARCH ARTICLE

Mechanosensitive miR-100 coordinates TGFβ and Wnt signaling in osteocytes during fluid shear stress

Neha S. Dole[1] | **Jihee Yoon**[1] | **David A. Monteiro**[1] | **Jason Yang**[2] | **Courtney M. Mazur**[1] | **Serra Kaya**[1] | **Cassandra D. Belair**[3,4] | **Tamara Alliston**[1,3]

[1]Department of Orthopaedic Surgery, University of California, San Francisco, San Francisco, California, USA

[2]Department of Molecular & Cell Biology, University of California Berkeley, Berkeley, California, USA

[3]Eli and Edythe Broad Center of Regeneration Medicine and Stem Cell Research, University of California, San Francisco, San Francisco, California, USA

[4]Department of Urology, University of California, San Francisco, San Francisco, California, USA

Correspondence
Tamara Alliston and Neha S. Dole, Department of Orthopaedic Surgery, University of California, San Francisco, 513 Parnassus Avenue, S1155 San Francisco, CA 949041, USA.
Email: Tamara.Alliston@ucsf.edu and NehaShashank.Dole@ucsf.edu

Funding information
NIAMS, Grant/Award Number: R21 AR067439 and P30 AR066262-01; NIH-NIDCR, Grant/Award Number: R01 DE019284; Office of Research on Women's Health, Grant/Award Number: 1636331; Department of Defense, Grant/Award Number: PRORP OR130191

Abstract

Organism scale mechanical forces elicit cellular scale changes through coordinated regulation of multiple signaling pathways. The mechanisms by which cells integrate signaling to generate a unified biological response remains a major question in mechanobiology. For example, the mechanosensitive response of bone and other tissues requires coordinated signaling by the transforming growth factor beta (TGFβ) and Wnt pathways through mechanisms that are not well-defined. Here we report a new microRNA-dependent mechanism that mediates mechanosensitive crosstalk between TGFβ and Wnt signaling in osteocytes exposed to fluid shear stress (FSS). From 60 mechanosensitive microRNA (miRs) identified by small-RNAseq, miR100 expression is suppressed by in vivo hindlimb loading in the murine tibia and by cellular scale FSS in OCY454 cells. Though FSS activates both TGFβ and Wnt signaling in osteocytes, only TGFβ represses miR-100 expression. miR-100, in turn, antagonizes Wnt signaling by targeting and inhibiting expression of Frizzled receptors (FZD5/FZD8). Accordingly, miR-100 inhibition blunts FSS- and TGFβ-inducible Wnt signaling. Therefore, our results identify FSS-responsive miRNAs in osteocytes, including one that integrates the mechanosensitive function of two essential signaling pathways in the osteoanabolic response of bone to mechanical load.

KEYWORDS
fluid shear stress, mechanobiology, microRNA, osteocytes, TGFβ, Wnt

Abbreviations: BMP, bone morphogenetic protein; BMSCs, bone marrow stromal cells; DAAM1, dishevelled associated activator of morphogenesis; ECM, extracellular matrix; FSS, fluid shear stress; FZD, frizzled receptors; GSK-3β, glycogen synthase kinase; LCN, lacuno-canalicular network; MAPK, mitogen-activated protein kinase; miR, microRNA; OPG, osteoprotegerin; PI3K/AKT, phosphoinositide 3-kinase/protein kinase B; Ptgs2, prostaglandin-endoperoxide synthase 2; RANKL, receptor activator of NF-κB ligand; SOST, sclerostin; TGFβ, transforming growth factor beta.

1 | INTRODUCTION

Through our daily activities, our bodies encounter multiple mechanical forces of varying magnitude, frequency, and duration.[1–3] Perhaps more so than any other organ system, the skeleton is literally shaped through the biological interpretation of mechanical forces, from early in development throughout vertebrate life.[4–7] Conversely, the absence of mechanical forces in microgravity or perturbations to the mechanotransduction pathways that sense and respond to these physical cues cause significant dysfunction in the skeleton and in other tissues.[8,9] The skeleton relies on bone-embedded osteocytes to convert these physical cues into a multitude of biological signals that guide tissue-level outcomes such as bone deposition or resorption.[10] However, many questions remain about the mechanisms by which cells generate a coordinated biological response to changing mechanical demands.

In bone, macroscale mechanical forces induce deformations that stimulate the flow of interstitial fluid through the porous lacunocanalicular network that houses osteocytes.[11,12] This fluid flow shear stress (FSS) in osteocytes then initiates a cascade of signaling events, which ultimately promotes bone formation and suppresses bone resorption. Osteocytes respond to FSS through several mechanisms, including activation of ion channels, integrin-mediated signaling at focal adhesions, and G-protein coupled receptor signaling, among others.[8,13,14] FSS instigates an acute surge in intracellular calcium and ATP release that trigger second messengers like nitric oxide and prostaglandins to modulate multiple cellular signaling pathways, including transforming growth factor beta (TGFβ) and canonical Wnt/β-catenin signaling.[15–23] Accordingly, FSS-treated osteocytes possess increased levels of phosphorylated Smad3 and active β-catenin, canonical effectors of the TGFβ and Wnt pathway, respectively. TGFβ and Wnt signaling act in parallel, but exert distinct effects on osteocyte behavior.[15,24–28] Both TGFβ and Wnt signaling are required for bone to generate the robust anabolic response to applied mechanical loads, and as such are attractive targets of therapies to prevent bone fragility. In spite of the importance of understanding TGFβ and Wnt signaling in osteocytes, it is unclear how the activity of these and other essential mechanoresponsive pathways are coordinated to generate an integrated cellular response to FSS. Since microRNAs (miRNAs, miRs) are have been recognized as powerful modulators that temporally regulate multiple pathways and cellular processes, we aimed to identify the FSS-regulated mechanosensitive miRs in osteocytes.

Recently, miRNAs have gained recognition as global fine tuners that can regulate an entire landscape of cellular gene expression, integrating multiple signaling cascades to generate a unified and unique biological response.[29,30] As short non-coding single stranded RNAs, miRs regulate endogenous gene expression by binding to mRNAs with sequence complementarity to the 'seed region'. Once bound to the target mRNAs, miRs post-transcriptionally inhibit target gene expression via direct degradation of target mRNA, and/or through suppression of translation.[31] In this way, miRs integrate signaling responses to diverse biochemical and physical cues to generate a unified and unique biological response. Mechanosensitive miRs have been reported to dramatically alter the cellular transcriptome and signaling profile of vascular endothelial cells and cardiomyocytes in response to physical cues.[32–34] In bone, miRNAs regulate multiple processes, including embryonic bone development and post-natal bone homeostasis.[35–39] In pre-osteoblasts, miRs participate in fluid shear stress-induced osteogenic differentiation; and several miRs that are sensitive to various mechanical stimuli guiding osteogenic differentiation and bone formation have been revealed.[40–42] Although osteocytes are the primary mechanosensitive cell type in bone, fluid shear stress-responsive mechanosensitive miRs in osteocytes are yet to be elucidated. Therefore, we hypothesized the existence of a miR-dependent mechanism in coupling the osteocyte response to FSS and coordinating changes in multiple osteocytic signaling pathways that are required for the anabolic response of bone to mechanical load.

In this study, we conducted a comprehensive profiling of mechanosensitive miRs in OCY454 osteocyte-like cells subjected to FSS. Our systematic analysis led us to focus on a candidate miR-100, whose expression was down-regulated with fluid shear stress as well as with compressive bone loading. We demonstrate that miR-100 is a negative regulator of canonical Wnt signaling that mediates crosstalk between Wnt and TGFβ pathways in osteocytes. Therefore, miR-100 is a crucial component of osteocyte mechanotransduction machinery that integrates TGFβ and Wnt signaling, and likely participates in the integrated anabolic response of bone to mechanical load.

2 | MATERIALS AND METHODS

2.1 | Cell culture, differentiation, transfections, and treatments

MLO-Y4 osteocyte-like cells (gift from L. Bonewald) were maintained in α-minimum essential medium (α-MEM, Gibco, Life Technologies) supplemented with 2.5% fetal bovine serum (FBS, Hyclone, Gibco), 2.5% bovine calf serum (Hyclone, Gibco), and 1% penicillin-streptomycin.[43]

OCY454 osteocyte like cells (gift from P. Divieti Pajevic) were grown on collagen-coated (0.15 mg/ml

type I collagen; Corning) dishes with α-MEM containing 10% FBS and 1% antibiotic–antimycotic (Gibco, Life Technologies). OCY454 cells were seeded and allowed to reach 80% confluency at the permissive temperature (33°C) before an experiment or passaging.[28]

For differentiation of primary bone marrow stromal cells (BMSCs) to osteoblasts and osteocytes, BMSCs were harvested from femurs and tibiae of 8-week-old C57BL6 male mice and cultured for 6 days in media containing α-MEM and 10% FBS. At the first passage, cells were replated at 150 000 cells/well in 6-well plates, grown to confluence, and differentiated for 3 weeks. Differentiation was accomplished in the presence of 5 mM β-GP and 50 μg/ml ascorbic acid; and media was changed every 3 days. Cells were harvested at 1 and 2 weeks of differentiation for isolation of RNA.

OCY454 cells (1×10^5), seeded on 6-well plates and cultured overnight, were transfected with 50–100 nM miR-100 inhibitor (miR-100I, AM17000, Assay ID: AM10188) or a negative control anti-miRNA (CI) inhibitor (CI, AM17010) purchased from ThermoFisher Scientific. Transfection was performed using Lipofectamine 3000 according to the manufacturer's instructions (Life Technologies, USA). To modulate the TGFβ pathway, OCY454 cells were cultured in growth media supplemented with either exogenous TGFβ1 ligand (5 ng/ml, Peprotech, Cat# AF-100-21C) or SB-431542, a TβRI (ALK4/5/7) kinase inhibitor (10 μM, Selleckchem). To stimulate canonical Wnt/b-catenin signaling, cells were treated with either Wnt3a ligand (50 ng/ml, Peprotech, Cat# 315-20) or CHIR99021, a GSK3 inhibitor (10 μM, Abcam, Cat# ab120890). Cells were cultured in low serum media (α-MEM containing 0.5% fetal bovine serum) for 1 h prior to and during treatment in order to generate a more synchronous response to exogenous ligand stimulation. Following these treatments, cell lysate was collected for luciferase or western analysis, or RNA was collected for qRT-PCR or RNA-seq analysis.

2.2 | Fluid shear stress

For exposure to FSS, OCY454 cells were plated in validated, custom microfluidic devices coated with rat tail collagen type I solution (CB-40235, Corning).[27] Cells seeded at 1×10^6 cells/ml in each microfluidic chamber were allowed to grow for 24 h at the permissive temperature (33°C). Cells were cultured in low serum media (α-MEM containing 0.5% fetal bovine serum) for 1 h prior to and during FSS exposure. Using a peristaltic pump (NE-1800, New Era Pump Systems) that was installed in a sterile incubator for continuous circulation of media, cells were exposed to 10 dynes/cm^2 of FSS. For most experiments, FSS was applied for 1 h, followed by a 1-h recovery. For small RNA seq, cells were subjected to FSS for 2 h, and total RNA was collected 8 h post-flow. This specific time regimen was selected based on previous findings that maximal transcriptomic changes in FSS-stimulated osteocytes are detected after an 8-h recovery period.[44] For all FSS experiments, static conditions correspond to cells grown in microfluidic chambers but not stimulated with FSS.

2.3 | Tibial compression loading

All animal procedures were approved by the Institutional Animal Care and Use Committee of the University of California San Francisco. Axial compressive loads were applied to the tibia using a Bose Electroforce ELF3200 desktop load frame (Bose, MN, USA) fitted with two custom-made hemi-spherical fixtures that gripped the mouse knee and ankle.[45] At eight weeks of age, male C57BL/6 mice were anesthetized with ketamine-xylazine and subjected to one session of axial compressive loading. Each loading session consisted of 600 cycles of a 1 Hz sinusoidal waveform applied with a preload of 0.5 N and maximum force of upto 6 N. Ex vivo calibration using in situ strain rosettes found that these loading parameters produce maximum tensile strains of approximately 1200 με on the anteromedial surface of the tibia at 37% of the bone length from the proximal end. For each mouse, only the right hindlimb was loaded (L), while the left hindlimb was not loaded to serve as the contralateral control (non-loaded, static).[46] From mice euthanized 24 h later, loaded and non-loaded tibias were dissected to remove epiphyses, soft tissues, and periosteum. Bone marrow was removed by centrifugation at 9000 rpm for 30 s at room temperature and bones were flash-frozen in liquid nitrogen and homogenized using a polytron in QIAzol lysis reagent (Qiagen, Life Technologies) for RNA isolation.[47,48]

2.4 | Total RNA isolation and small RNA-seq

Following homogenization, RNA was purified from bone using an miRNeasy minikit (Qiagen, Cat# 217004) that captures both small and messenger RNA.[49,50] For superior yields, cellular RNA from OCY454 cells subjected to static and FSS culture conditions was obtained by QIAzol mediated cell lysis and through precipitating, purifying, and concentrating RNA using the miRNeasy microkit (Qiagen, Cat# 217084). All RNAs were subjected to on-column DNase treatment to minimize genomic DNA contamination (Qiagen, Cat# 79254). Three to four biological replicates were collected for each condition and/or treatment. RNA concentration was determined by nanodrop

and the quality of total RNA as well as the small RNA (<150 bp) was assessed using the Bioanalyzer RNA 6000 Pico kit (Agilent, Cat# 5067-1513).

Small RNA-seq libraries were made as described in Ref. [51]. Briefly, 500 ng of total RNA was used as input for generating libraries. Sequencing adapters were synthesized by Integrated DNA Technologies.[51] Three prime adapters were used at 1 μM while 5′ adapters were added at 0.1 μM. Fragments of the 45–50 bp size were PAGE purified after each ligation step, reverse transcribed, and then PCR amplified. Unless otherwise noted, PCR was performed for 12 cycles. The generated library was quantified using Qubit2 and diluted to 3–10 nm concentration prior to sequencing on Illumina HiSeq 2000 sequencers.

Raw reads were quality checked with the FASTQC package (version 0.11.2) and processed using CutAdapt v1.8 (doi:10.14806/ej.17.1.200) to trim adapters. Sequences were then aligned using Bowtie v1.1.2 to a mature miRNA and other small RNA genome, downloaded from miRbase and the mouse genome index curated by the GENCODE annotations (Release M25 (GRCm38.p6) at https://www.gencodegenes.org/releases/current.html). Reads were mapped sequentially to first remove all sequences inherent to library production (i.e., adapters, markers, PhiX), followed by mapping mature miRNA and then other small RNA to the mouse genome. Differentially expressed (DE) genes were analyzed using DESeq2 package (v.1.24.0) (doi:10.1186/s13059-014-0550-8) and a cut-off for significantly different genes was set to a false discovery rate of 0.05. The heatmap was generated using the pheatmap package (v.1.0.12) in R with Euclidean clustering method. Normalized miRNA reads were transformed into relative abundance data by dividing each individual miRNA count by the total miRNA counts in each sample. The average read across of the 4 biological replicates was calculated and ranked to determine which miRNAs were most abundant.

2.5 | qRT-PCR

miR-100 levels were quantified using the TaqMan MicroRNA assay (Life Technologies, Grand Island, NY, USA). miRNA levels were normalized to small nuclear RNA snoRNA 202, which is recommended as an endogenous control for mice.[52] For Fzd-4, Fzd-5, Fzd-8, Tcf-4, Axin-2, and Lef-1, expression was normalized to 18S ribosomal RNA using TaqMan Gene Expression Assays (Life Technologies). The catalog number of the primers used in this study is provided in Table S2. PCR was conducted following the recommendations for the TaqMan Gene Expression Assays on a CFX96 Real-Time PCR System (Bio-Rad). The fold change for each miRNA and mRNA relative to the control was calculated using the ΔΔCt method.[53,54] qRT-PCR data are reported as either mean ± SD for FSS and loading experiments or as mean ± SE when data are derived from 3 independent experiments, with $n = 3$–4 biological replicates/group and an average of two technical replicates for each experiment.

2.6 | Western blot analysis

Whole cell lysates were collected and processed as previously described.[28] Proteins were resolved by 10% SDS–PAGE and transferred onto polyvinylidene fluoride membranes. Membranes were blocked with 5% milk in Tris-buffered saline with 0.1% Tween 20 and then incubated with primary antibodies against mouse FZD-8 (1:1000, Abcam ab155093), active β-catenin (1:1000, Cell Signaling D13A1, Cat# 8814), GSK-3β (1:1000, Cell Signaling 27C10, Cat# 9315), and p-GSK-3β (1:1000, Cell Signaling, Cat# 9336), followed by an anti-rabbit secondary antibody conjugated to IRD Dye 800 CW (1:5000; LI-COR Biosciences), and visualized using the Odyssey Imaging System. β-actin levels were used as a normalizing control for protein loading. The expression of β-actin was detected using anti-β-actin (1:2500, Abcam ab8226) primary antibody and an anti-mouse secondary antibody conjugated to IRD Dye 700 CW (1:15 000; LI-COR Biosciences). All of the western assays were conducted with at least 3 biological replicates per group from at least 2–3 independent experiments. The results of protein expression were quantitatively analyzed with Image Studio Lite software and presented as the mean ± SD and the graphs are a representative of 3 independent experiments.

2.7 | Luciferase reporter assay

The reporter plasmids TOPFlash containing wild-type TCF/LEF DNA binding sites (CCTTTGATC; Addgene plasmid # 12456) or FOPFlash containing mutated TCF/LEF DNA binding sites (CCTTTGGCC; Addgene plasmid # 12457) were purchased from Addgene.[55] For luciferase reporter assays, OCY454 cells seeded at 3×10^4 cells/well in 24-well plates were grown to 70%–80% density. Cells were then transfected with either TOPFlash or FOPFlash reporters (1 mg), in combination with either miR-100 or scrambled control inhibitors (CI) (50 nM) using Lipofectamine 3000 (Invitrogen). As a control, cells were co-transfected with 100 ng of beta-galactosidase plasmid. Eighteen hours post-transfection, cells were treated with CHIR99021 (10 μM, Abcam# ab120890) or Wnt3a (50 ng/ml, Peprotech# 315-20) for 24 h and cell lysate was collected for the luciferase and beta-galactosidase assay according

to the manufacturer's instructions (Galacto-Light Plus™ β-Galactosidase Reporter assay-ThermoFisher Scientific). The luciferase reporter assays were conducted with 5–6 biological replicates per group in three independent experiments. Results are presented as the mean ± SD and data representative of 3 independent experiments are shown.

2.8 | miR-100 target prediction, cloning, and validation

miRNA target genes were predicted using miRsystems, a database that combines seven well-known miRNA target prediction programs into one: miRanda, PicTar, DIANA, miRBridge, rna22, PITA, and TargetScan.[56] Using this prediction tool, we selected 5 mRNAs to validate as targets of miR-100. The selection criteria for target validation were based on the mismatch within and outside the seed regions and the minimum free energy of the miR/target duplex. The 3′ UTRs of FZD4, FZD5, FZD8, SOST, and DAAM1 were amplified from the mouse genomic DNA using primers specified in Table S2. PCR amplification was performed in a 50 μL reaction mixture with the following cycling parameters: 1 min at 98°C, followed by 40 cycles of denaturation at 98°C for 10 s, annealing for 30 s, and extension at 72°C for 30 s, and a final extension step at 72°C for 5 min. The amplification products were cloned into the psiCHECK2 vector (C8021, Promega) multiple cloning site using NotI and XhoI restriction sites. The constructed 3′ UTR luciferase reporters were sequenced to verify the base sequence of miR-100 binding sites. The psiCHECK-2 vector was selected because it contains both a renilla luciferase and an independently transcribed firefly luciferase reporter gene, which can be used for normalization purposes to account for variation in transfection efficiency and cell viability.

OCY454 cells seeded at 1×10^4 cells/well density in 96-well plates were transfected with 100 ng of the relevant psiCHECK2 3′ UTR reporter constructs (psiCHECK2-FZD4-3′ UTR, psiCHECK2-FZD5-3′ UTR, psiCHECK2-FZD8-3′ UTR, psiCHECK2-SOST-3′ UTR, psiCHECK2-DAAM1-3′ UTR) and 50 nM miR-100 or CI inhibitors using Lipofectamine 3000 (Invitrogen). Lysates were harvested 48 h after transfection and Firefly and Renilla Luciferase signals were measured using the Dual Luciferase Reporter Assay Kit (Promega, USA), according to the manufacturer's protocol. Renilla luciferase signal (that is upstream of the cloned 3′ UTR) was normalized to firefly luciferase signal and the normalized ratio was compared between samples and using the independent sample *t*-test. All of the luciferase reporter assays were conducted with 5–6 biological replicates per group in three independent experiments and data representative of 3 experiments is reported.

2.9 | Statistical analysis

Analyses were performed using GraphPad Prism. A two-tailed Student's *t* test was used to evaluate the statistical significance of the differences between two groups. One-way analysis of variance (ANOVA) was used to compare the differences among three or more groups followed by Holm-Šídák's post hoc test. Probability values $<.05$ were considered statistically significant.

3 | RESULTS

3.1 | Differential expression of miRNAs in osteocytes with FSS

To identify FSS induced changes in the osteocyte miRNA transcriptome, we performed small RNA-seq using FSS-stimulated OCY454 osteocyte-like cells. We first validated the mechanosensitive response of OCY454 cells to FSS grown in established microfluidic devices.[27] As expected, an hour of FSS was sufficient to stimulate a 3-fold increase in AKT phosphorylation (Figure 1A,B) and a 30-fold induction in *Ptgs2* (*Cox2*) mRNA expression (Figure 1C), relative to cells grown in microfluidic devices in static conditions.

The miR expression profile of OCY454 cells exposed to 2 h of FSS, followed by an 8-h recovery, was clearly segregated from cells grown in static conditions, as shown by principal component analysis (Figure 1D). DESeq2 identified 61 miRNAs that are DE in response to FSS, with a false positive rate of less than 5%. As shown in the heatmap (Figure 1E), the DE miRs were robustly different between static and FSS-subjected samples, with 32 FSS-induced and 29 FSS-repressed miRNAs (Figure 1F). Figure 1G shows the distribution of 11 most abundant miRNAs, miR-351-5p, miR-5099-5p, miR-100-5p, miR-148a-3p, miR-182-5p, miR-199a-5p, miR-151-3p, miR-24-3p, miR-16-5p, miR-191-5p, and miR-92a-3p, which account for more than 85% of reads for both the static and FSS groups. In response to FSS, these abundantly expressed miRNAs are induced or repressed by greater than 30% (Figure 1H). A 30% change in the expression levels of these abundant miRs in response to FSS is sufficient to exert a significant influence on gene regulation and cellular function.[57] To predict the effect of their differential expression on osteocytes, we used miRsystems, a web-based bioinformatics tool that integrates several prediction databases (TarBase, DIANA, miRanda, mirBridge, PicTar, PITA, RNA22, and

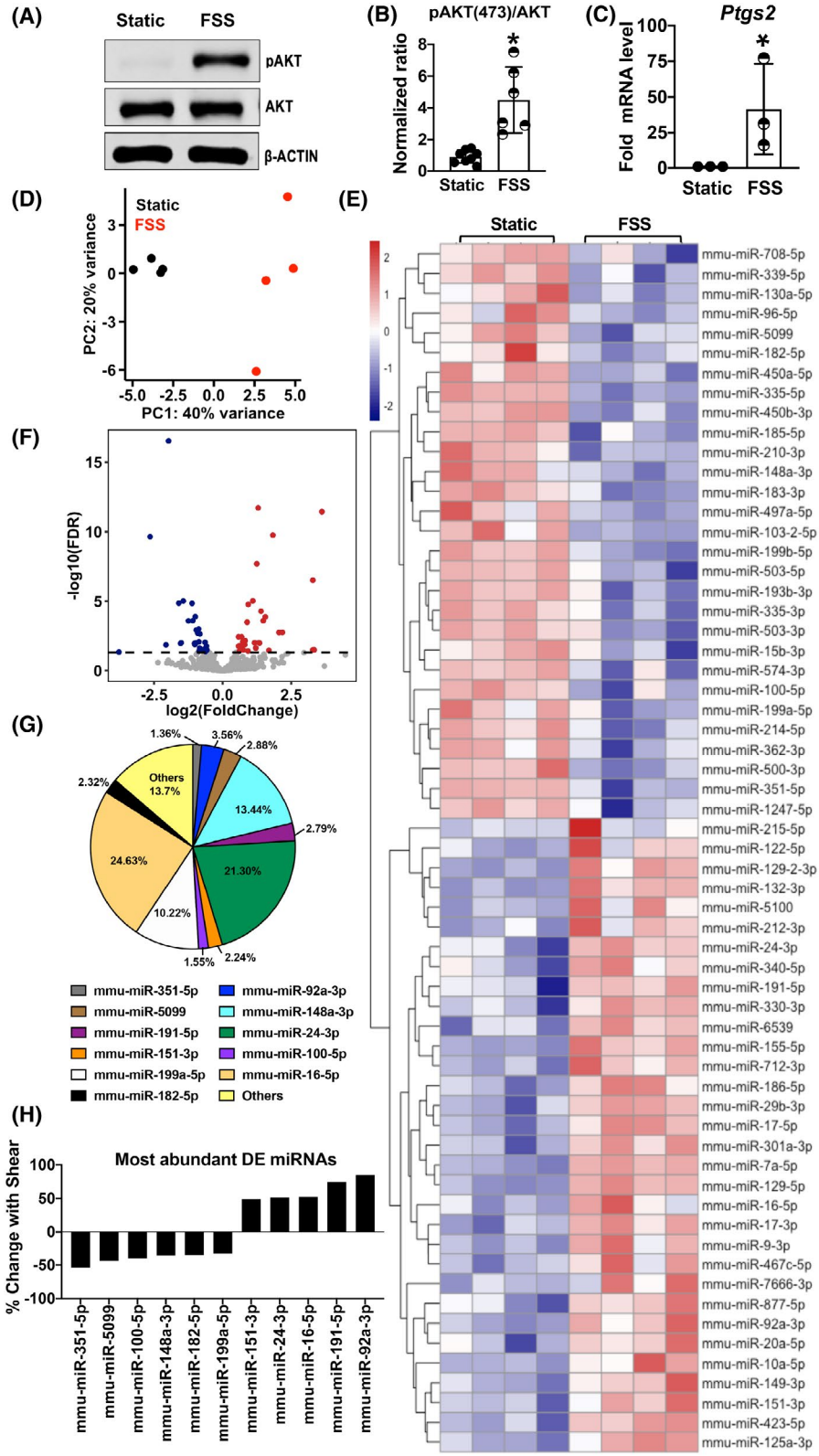

TargetScan, http://mirsystem.cgm.ntu.edu.tw/index.php).[56] Several pathways that are well-known to participate in mechanotransduction are predicted targets of these 11 abundant miRs, including focal adhesion, actin cytoskeleton, canonical Wnt, TGFβ, Mapk, and Notch signaling pathways (Figure S1).

For detailed characterization of miRNA function in osteocyte mechanotransduction, we deliberated on the literature to select a miRNA candidate that has an established role in bone physiology and is associated with clinically relevant bone pathologies, as shown in Table 1. These strict selection criteria prioritized miR-100 as an excellent

FIGURE 1 Fluid shear stress regulates microRNAs in OCY454 osteocyte-like cells. Undifferentiated OCY454 cells grown in microfluidic flow chambers, under static conditions or subjected to fluid shear stress (FSS) at 10 dynes/cm^2 for 60 min, exhibit induction in Akt phosphorylation on Ser473 (pAKT) with FSS. Protein levels of pAKT and total AKT are normalized to β-actin (A and B) and ratio of phosphorylated to total AKT is quantified ($n = 6$ replicates/group, mean ± SD). FSS induced upregulation of *Ptgs2* mRNA levels (C), quantified with qRT-PCR ($n = 3$ replicates/group, data derived from 3 experiments are shown as mean ± SEM). Mechanosensitive microRNAs are profiled using an unbiased small RNA-seq on RNA collected from OCY454 cells subjected to 2 h of 10 dynes/cm^2 FSS, followed by 8-h recovery. A principal component analysis plot (D) demonstrates segregation of the four biological replicates between the static and FSS conditions. Of the 650 miRs detected by the small RNA seq, 61 differentially expressed (FDR < 0.05) miRs are shown in a heatmap (E). Each row of the heatmap represents the log2FC value of one differentially expressed gene across all samples (column) and the dendrograms are constructed by the Euclidean distance. Red shading indicates higher expression whereas blue shading indicates lower expression. Volcano plot (F) shows significantly differentially expressed miRs, (FDR < 0.05); red denotes upregulated, while blue denotes downregulated, miRs. The 11 most abundant miRs account for 87% of the total detected reads (G) and the percent change in the read counts of these abundant miRs with FSS is shown graphically (H). *$p < .05$ compared to static group, unpaired *t*-test

TABLE 1 Mechanosensitive regulation of abundant DE miRs and their known roles in bone

miRNAs	Function	Clinical relevance	Mechano-sensitive miRs
miR-351-5p	Inhibitor of bone formation[62]	Unknown	Yes
miR-5099	Unknown	Unknown	Unknown
miR-100-5p	Inhibitor of osteoclastogenesis and osteoblastogenesis[58,59]	Upregulated in osteoporosis, osteoarthritis, and osteonecrosis[60,61,63,64]	Yes[65]
miR-148a-3p	Inhibits osteogenesis[66]	Upregulated in osteoporosis[60]	Yes[67]
miR-182-5p	Inhibitor of osteoblast proliferation and differentiation[68]	Unknown	Unknown
miR-199a-5p	Promoter of bone formation[69]	Unknown	Yes[70]
miR-151-3p	Unknown	Osteopenia and fracture healing diabetes[71,72]	Unknown
miR-24-3p	Unknown	Upregulated in osteoporosis[60,73]	Unknown
miR-16-5p	Unknown	Postmenopausal osteoporosis[74]	Yes[75]
miR-191-5p	Unknown	Unknown	Yes[76]
miR-92a-3p	Promotes chondrogenesis[77]	Unknown	Unknown
miR-17-5p	Inhibits bone formation, targets BMP2, SMAD5, SMAD7 targets	Biomarker of osteoporosis	Yes[33]

candidate that is known to participate in various biological processes, including osteogenic differentiation and osteoclastogenesis.[58,59] miR-100 participates in ovariectomy-induced osteoporosis and is associated with increased risk of osteoporotic fracture in humans.[60,61] However, the role of miR-100 in osteocytes and mechanotransduction was unexplored.

3.2 | Expression of miR-100, an inhibitor of osteogenic differentiation, is mechanosensitive

miR-100 is a member of the miR-99 family that can suppress BMP2-induced osteogenic differentiation of C3H10T1/2 osteogenic precursors.[58] To determine its potential role in osteocytes, we examined miR-100 expression throughout osteocyte differentiation in mouse bone marrow stromal cells. While the expression of osteocyte markers, namely Dentin matrix protein 1 (*Dmp1*), Pododplanin (*Pdn*), Phosphate Regulating Endopeptidase Homolog X-Linked (*Phex*) and Sclerostin (*Sost*) increased over the 3-week differentiation period (Figure S2A), miR-100 levels declined by 40% during this time (Figure S2B). Similarly, miR-100 expression declines throughout osteoblast differentiation in the MC3T3E1.4 cell line (Figure S2C,D). Consistent with prior reports,[58] miR-100 inhibition is sufficient to stimulate a 10-fold increase in *Runx2* expression and a 4-fold increase in expression of *Oc* and *Ibsp* (Figure S2E–G). Given that miR-100 levels decline throughout and antagonize osteogenic differentiation, in mature osteocytes that are derived from

terminally differentiated osteoblasts, the repression of miR-100 is sustained.

Although miR-100 inhibits osteoblast differentiation (Ref. [58] and Figure S2E–G), the extent to which it participates in osteocyte mechanotransduction is unclear. In OCY454 cells subjected to FSS, qRT-PCR analysis showed a 50% reduction in miR-100 expression, similar to what was observed in our small RNA-seq results (Figure 2A). In vivo hindlimb loading of mice also suppressed miR-100 expression in osteocyte enriched bone RNA, relative to the contralateral non-loaded limb, further strengthening our conclusion that miR-100 is a mechanosensitive miRNA (Figure 2B).

3.3 | miR-100 expression is regulated by TGFβ, but not Wnt signaling

One of the major questions in mechanobiology is the identity of mechanisms by which cells integrate physical and biochemical stimuli to generate a coordinated response. To determine if the mechanosensitive miR-100 fulfills this function in osteocytes, we examined miR-100 regulation by TGFβ and Wnt signaling, two pathways that are sensitive to FSS and are integral to the anabolic response of bone to mechanical load. Using OCY454 cells treated with TGFβ for 24 h, we assessed expression of miR-100 and the established TGFβ-inducible gene, *Serpine1*. TGFβ treatment

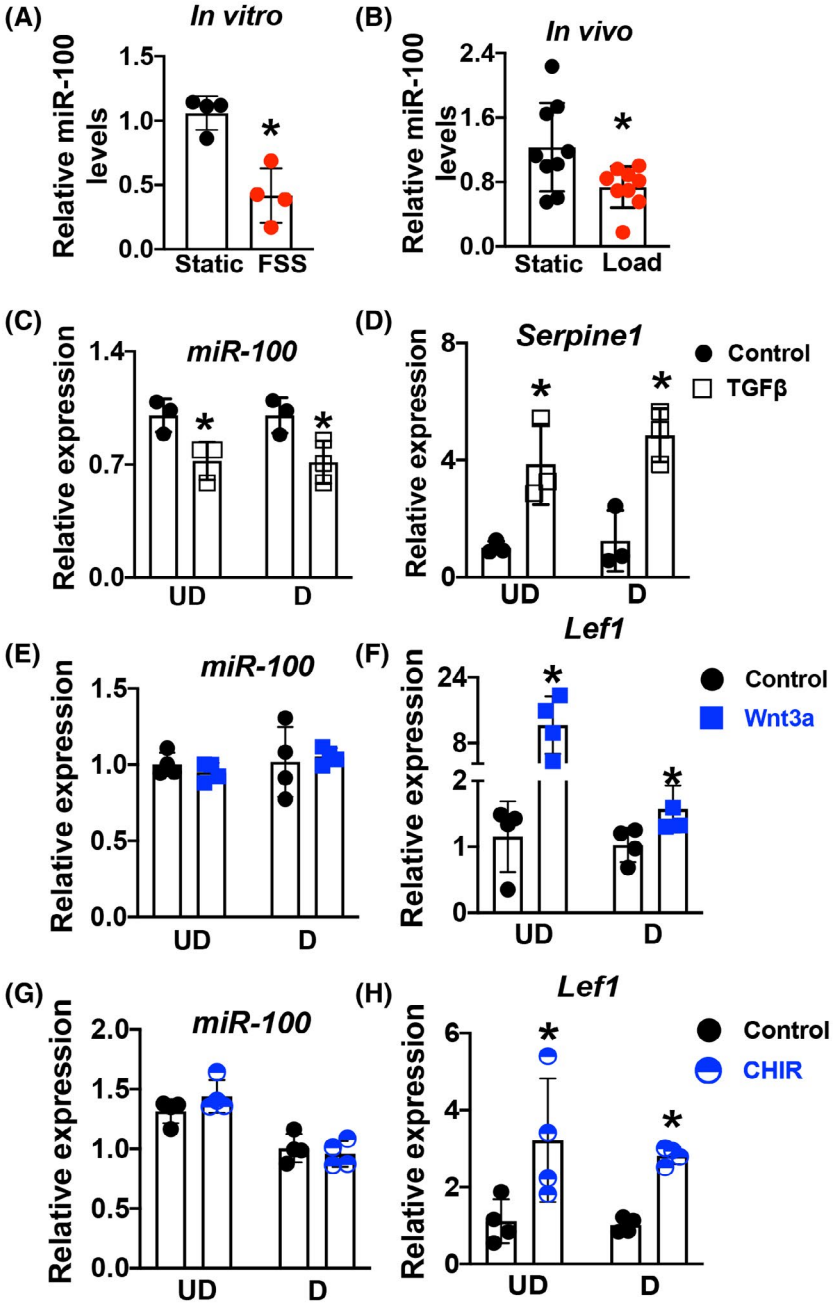

FIGURE 2 Mechanosensitive miR-100 is suppressed by TGFβ, but not Wnt, signaling. qRT-PCR showed that miR-100 expression was reduced by FSS (A) in cultured OCY454 cells ($n = 4$ replicates/group, mean ± SD) and by compressive hindlimb loading (B) in tibial bones when compared to the non-loaded (static) contralateral tibia from same mouse ($n = 9$ mice/group, mean ± SD). In undifferentiated (UD) and differentiated (D) OCY454 cells, 24-h treatment with TGFβ treatment (5 ng/ml, C and D) reduces miR-100 expression and induces the TGFβ-responsive gene, *Serpine1*, while treatment with Wnt3a (50 ng/ml, E and F) or the Wnt agonist, CHIR (10 μM, G and H), does not impact miR-100 expression, despite upregulating the expression of Wnt-responsive gene, *Lef1* ($n = 3$–4 replicates/group, mean ± SD, and data are representative of 3 experiments). snoRNA 202 and 18S ribosomal RNA were respectively used a endogenous housekeeping genes for normalizing miRNA and mRNA levels. *$p < .05$ compared to static or treatment controls, unpaired *t*-test

reduced miR-100 levels by 20% in both undifferentiated and differentiated osteocytes (Figure 2C), while increasing *Serpine1* mRNA levels by approximately 4-fold (Figure 2D). Similarly, in MLO-Y4 osteocyte-like cells, TGFβ repressed miR-100 expression; and this repression was relieved in the presence of an inhibitor of TGFβ pathway, SB431542 (Figure S2H,I). In contrast to TGFβ, treatment with Wnt3a or CHIR, a GSK3β inhibitor that activates the Wnt pathway, miR-100 expression was unaffected (Figure 2E,G). Activation of Wnt signaling with Wnt3a and CHIR was confirmed in osteocytes by detecting elevated mRNA levels of Lef1, a Wnt-inducible target gene (Figure 2F,H).

3.4 | miR-100 regulates Wnt/β-catenin pathway in osteocytes

Since miR-100 is a downstream target of FSS and TGFβ, but not Wnt, we hypothesized that miR-100 acts upstream of Wnt signaling in osteocytes, as it does in cancer and in hematopoietic cells.[78,79] Further supporting the ability of miR-100 to target Wnt signaling, in-silico analysis with miRsystem scored several Wnt signaling genes, including Fzd4, Fzd5, Fzd8, Sost, and Daam1, as likely targets of miR-100 (Table 2). The complementarity of the miR-100 seed region to the 3′ UTR of several predicted target transcripts is shown in Figure 3A. To determine whether Fzd5, Fzd8, Sost, and Daam1 are bona fide miR-100 targets, psiCHECK2 luciferase reporter constructs were developed for the 3′-UTR of each gene. When transfected into OCY454 cells, constructs show a loss of luciferase signal if miR-100 targets the relevant 3′ UTR. Restoration of reporter activity upon co-transfection of miR-100 inhibitor validates the specificity. The luciferase activity of Fzd5, Fzd8, and Daam1 constructs was higher in the presence of miR-100 inhibitor compared to the non-targeting control inhibitor (CI), while the activity of the Sost 3′-UTR remained unaffected (Figure 3B). These data suggest that miR-100 directly targets Fzd5, Fzd8, and Daam1, but not Sost.

In OCY454 cells transfected with control and miR-100 inhibitors, we also examined the mRNA levels of Fzd5 and Fzd8, two receptors in the canonical Wnt pathway. Fzd5 and Fzd8 mRNA levels were significantly increased with miR-100 inhibition, but not in the control inhibitor containing cells (Figure 3C,D). Western analysis further showed more than 2-fold induction in FZD8 protein levels in the presence of miR-100 inhibitor compared to the non-targeting control group (Figure 3E,F). Apart from Wnt receptors, miR-100 inhibition also increased expression of the Wnt effector, β-Catenin, as demonstrated by increased mRNA (Figure 3G) and protein levels (Figure 3H,I). Ultimately, we examined the functional effect of miR-100 inhibition on the Wnt-responsive luciferase reporter TOPFlash, a construct with seven tandem copies of the consensus Tcf/Lef binding site, in OCY454 cells. CHIR mediated induction of TOPFlash reporter activity is augmented in the presence of miR-100 inhibitor, with approximately 6-fold higher reporter activity than control inhibitor transfected cells (Figure 3J). Together, these data demonstrate that miR-100 antagonizes Wnt signaling in osteocytes, as it does in other cell types,[78,79] at least in part, by reducing the expression of Wnt receptors.

TABLE 2 KEGG analysis using miRsystems revealed Wnt signaling among the top 10 pathways predicted to be targeted by miR-100

miR-100 targeted pathways	*p* value	Predicted gene targets
Pathways in cancer	.0001	PPP3CA; SMARCD1; SMARCC1; FZD5; FZD8; PPP2R5C; TNF; MTOR
Endocytosis	.0004	EEA1; VPS37C; AGAP3; FGFR3; IGF1R
Prostate cancer	.0007	E2F2; MTOR; IGF1R; NKX3-1
Mapk signaling	.0012	PPP3CA; TAOK1; TNF; FGFR3; IGF1R; MAP2K6; FGF21
Oocyte meiosis	.0015	PPP3CA; PPP2R5C; ADCY1; IGF1R
Amyotrophic lateral sclerosis	.0019	APP; FZD5; FZD8
Glioma	.0029	E2F2; MTOR; IGF1R
Adipocytokine signaling	.0033	ACSL4; TNF; MTOR
Melanoma	.0038	E2F2; IGF1R; FGF21
Wnt signaling	.0044	PPP3CA; FZD5; FZD8; PPP2R5C; DAAM1; SOST
Glycosaminoglycan biosynthesis	.0059	HS3ST3B1; HS3ST2
Tgf-beta signaling	.0061	BMPR2; FMOD; SMAD7
Melanogenesis	.0094	FZD5; FZD8; ADCY1

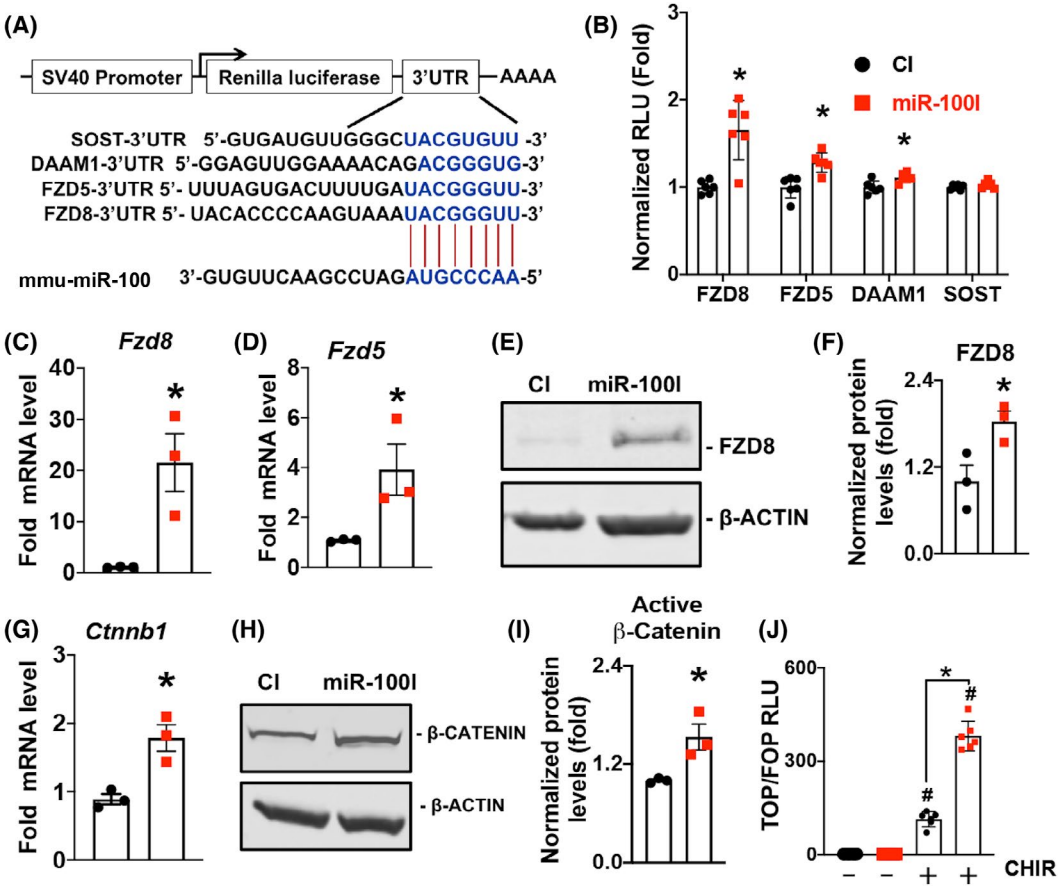

FIGURE 3 miR-100 directly targets multiple components of the Wnt/β-catenin signaling pathway. The 3′ UTR of FZD5 (seed region: 3721–3727), FZD8 (seed region: 508–514), DAAM1 (seed region: 461–473), and SOST (seed region: 409–415) contain putative miR-100 binding sites as shown in (A). Cloning into the psiCHECK-2 reporter showed that these 3′ UTR fragments of mouse FZD5, FZD8, and DAAM1, but not SOST, are sufficient to confer reporter sensitivity to miR-100. Normalized luciferase activity of 3′ UTR constructs (B) in OCY454 cells transfected with miR-100 Inhibitor (miR-100I) or control inhibitor (CI), are reported ($n = 6$ replicates/group, mean ± SD). OCY454 cells transfected with miR-100I (red) or CI (black) show miR-100 sensitivity of *Fzd5* (C) and *Fzd8* (D) mRNA levels ($n = 3$ replicates/group, data derived from 3 experiments are shown as mean ± SEM). Western blot (E and F) shows 2-fold increase in FZD8 protein levels, normalized to β-actin, in miR-100I transfected OCY454 cells, relative to CI ($n = 3$ replicates/group, mean ± SD). The inhibitory effect of miR-100 on Wnt signaling is evident from the increased expression of β-catenin *(Ctnnb1)* mRNA (G) and active β-catenin protein levels (H and I) ($n = 3$ replicates/group, for G data are shown as mean ± SEM and mean ± SD for I). Relative luciferase activity of TOPFlash/FOPFlash (J) in OCY454 cells co-transfected with miR-100I or CI and treated with vehicle or CHIR for 18–20 h ($n = 6$ replicates/group, mean ± SD). *$p < .05$ relative to the CI group and $^{\#}p < .05$ relative to the untreated CI group, One-way ANOVA followed by Holm-Šídák's post hoc test

3.5 | TGFβ activates Wnt/β-catenin signaling in osteocytes

Though TGFβ and Wnt signaling are induced by FSS, the mechanisms coordinating the activity of these pathways in osteocyte mechanotransduction remain unclear. Therefore, we further explored the crosstalk between these two pathways in osteocytes by examining the effect of TGFβ on Wnt signaling pathway at multiple levels. In OCY454 cells, 24 h of TGFβ treatment reduced *Axin2* mRNA levels by ~2.5-fold, while promoting expression of *Lef1* (~4-fold induction), a downstream target of canonical Wnt signaling (Figure 4A). TGFβ also reduced expression the mRNA levels of Wnt receptor *Fzd8*. To gain further clarity on the effect of TGFβ on Wnt pathway, we used the Wnt reporters (TOPFlash and FOPFlash). We observed that the combination of TGFβ and Wnt3a treatment doubled Wnt-inducible TOPFlash activity in transfected OCY454 cells (Figure 4B). Immunoblotting analysis revealed that TGFβ treatment (24-h) mediated increase in the active non-phosphorylated β-catenin protein levels were similar to those induced by Wnt 3a (Figure 4C,D). Also, TGFβ and Wnt3a in combination caused a significantly higher activation of β-catenin protein compared to either treatment alone. Interestingly, a 1-h long TGFβ treatment was found to suppress levels of active β-catenin, suggesting of multiple distinct mechanisms by which TGFβ

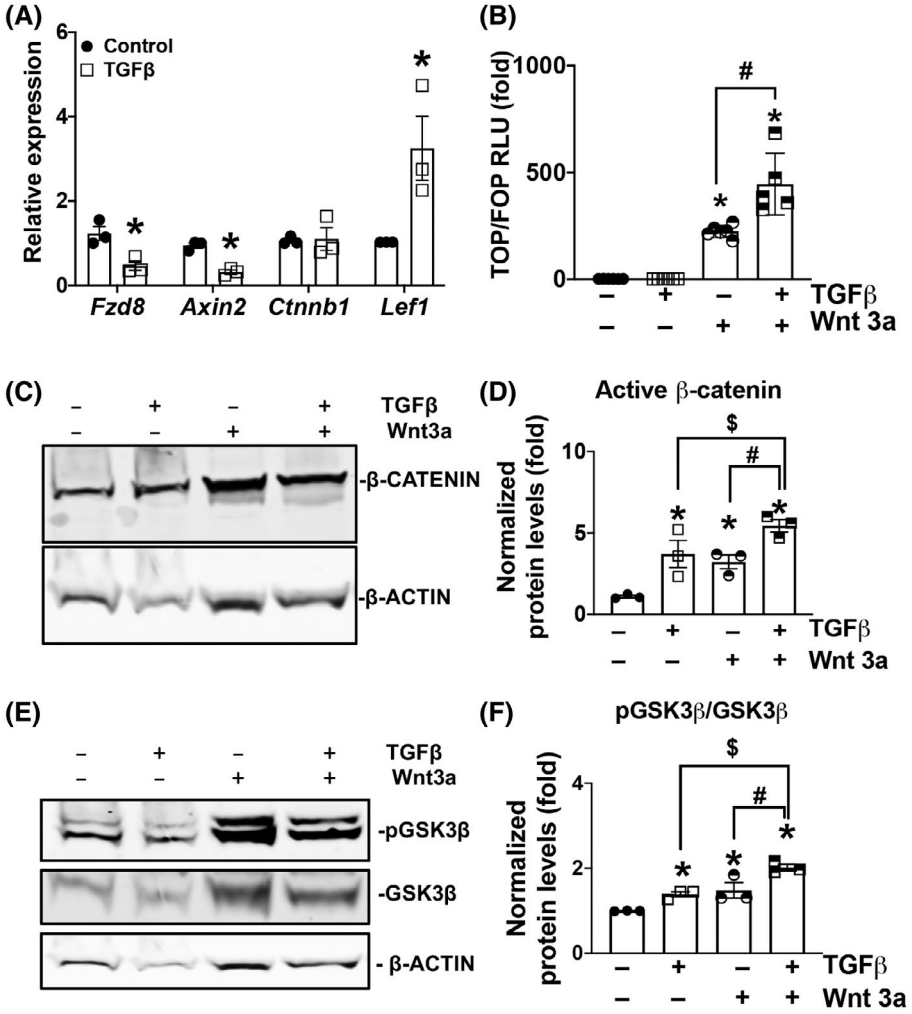

FIGURE 4 TGF-β increases osteocyte responsiveness to Wnt ligand. mRNA levels of *Fzd8*, *Axin2*, *Ctnnb1*, and *Lef1* (A) in OCY454s treated with TGFβ for 24 h are determined ($n = 3$ replicates/group, mean ± SEM). Relative luciferase activity (RLU) of Wnt reporter (TOPFlash/FOPFlash) (B) in OCY454 treated with or without TGFβ and Wnt3a ($n = 6$ replicates/group, mean ± SD). TGFβ and Wnt3a regulate the level of active β-catenin (C and D) and phosphorylated and total GSK3β (E and F), relative to β-actin, in OCY454 cells ($n = 3$ replicates/group, mean ± SD). $^{*}p < .05$ different from control group, $^{\#}p < .05$ different from Wnt3a group, and $^{\$}p < .05$ relative to TGFβ group, One-way ANOVA followed by Holm-Šídák's post hoc test

regulates Wnt pathway (Figure S3A). TGFβ treatment (24-h) was also found to induce phosphorylation of GSK3β on serine-9, which suppresses the Wnt-antagonizing function of GSK3β (Figure 4E,F). TGFβ treatment further augments Wnt3a-induced phosphorylation of GSK3β. Together these results provide evidence at multiple levels of the Wnt pathway and indicate that TGFβ acts in a cooperative manner to supplement Wnt/β-catenin signaling in osteocytes.

3.6 | miR-100 mediates cooperation between TGF-β and Wnt signaling

Since TGFβ suppresses miR-100 expression, and miR-100 antagonizes Wnt signaling, we sought to determine if miR-100 is necessary for TGFβ-induced Wnt/β-catenin activation in osteocytes. To test this hypothesis, OCY454 cells transfected with non-targeting control or miR-100 inhibitors were treated in the presence of TGFβ, Wnt3a, or both. Inhibition of miR-100 increased mRNA levels of *Ctnnb1* compared to the non-targeting control transfected cells (Figure 5A). TGFβ treatment resulted in a marked increase in *Ctnnb1* mRNA levels, comparable to the degree of *Ctnnb1* mRNA induction following Wnt3a treatment (Figure 5A). miR-100 inhibition augmented both TGFβ and Wnt3a-induced *Ctnnb1* mRNA expression. Levels of the Wnt downstream target, *Lef1* mRNA, were not substantially increased with TGFβ treatment; however, its addition augmented Wnt3a mediated increase in *Lef1* in both the presence and absence of miR-100 inhibitor. Inhibition of miR-100 substantially increased *Lef1* mRNA in presence of TGFβ and Wnt3a alone or in combination (Figure 5B).

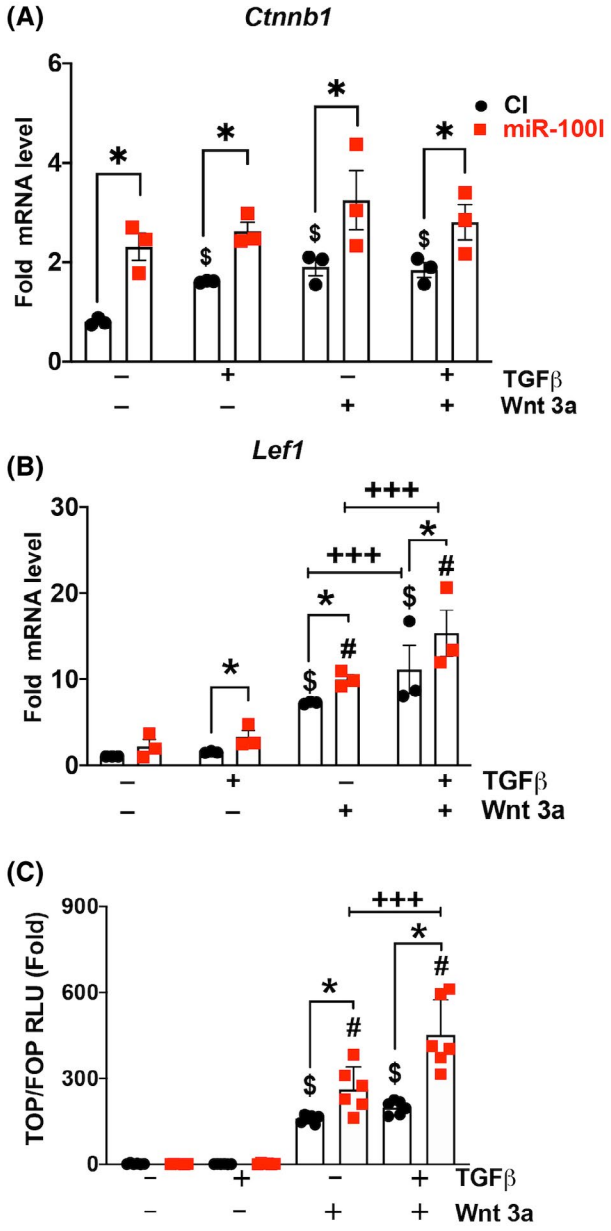

FIGURE 5 Cooperation between TGFβ and Wnt/β-Catenin signals is mediated in part by miR-100. The relative expression of Wnt target genes, *Ctnnb1* (A) and *Lef1* (B), in OCY454 cells is sensitive to TGFβ or Wnt3a treatment, applied 24 h post-transfection with CI or miR-100I is reported with qRT-PCR ($n = 3$ replicates/group, mean ± SEM). Relative luciferase activity (RLU) of Wnt reporter (TOPFlash/FOPFlash) (C) in OCY454 transfected with CI or miR-100I, treated with or without TGFβ and Wnt3a for 24 h is shown ($n = 6$ replicates/group, mean ± SD). $^{\$}p < .05$ different from the control treated and CI transfected group, $^{\#}p < .05$ different from the control treated and miR-100I transfected group, $^{*}p < .05$ different from the CI group, $^{+++}p < .05$ different from the Wnt3a treated group, One-way ANOVA followed by Holm-Šídák's post hoc test

As a functional measure of Wnt activity, we used the Wnt reporters (TOPFlash and FOPFlash) to determine if miR-100 is required for TGFβ-inducible Wnt signaling. In OCY454 cells transfected with non-targeting control inhibitor, Wnt-3a stimulated TOPFlash reporter activity by ~1.5 fold over the basal levels. Wnt3a stimulated an even greater induction when miR-100 inhibitors were present. Concomitant treatment of TGFβ significantly augmented Wnt-3a-inducible reporter activity, both in the presence or absence of miR-100 inhibitors. Remarkably, upon miR-100 inhibition, the combination of TGFβ and Wnt-3a induced reporter activity by ~2.3 fold (Figure 5C). Overall, this result suggests that TGFβ stimulation of Wnt signaling occurs, at-least in part, through inhibition of miR-100.

3.7 | miR-100-inhibition is sufficient to mimic FSS-inducible Wnt signaling

Lastly, we investigated if mechanosensitive suppression of miR-100 is sufficient to recapitulate the effect of FSS on Wnt signaling. As anticipated, we observed FSS-dependent regulation of canonical Wnt signaling using OCY454 cells grown in established microfluidic conditions (10 dynes/cm^2). Within 1-h of FSS, the outcomes of Wnt signaling, including GSK3β phosphorylation and Lef1 expression were induced (Figure 6A–C). FSS also caused a ~2-fold increase in active β-catenin protein levels, comparable to that induced by Wnt3a. Inhibition of miR-100 was sufficient to increase active β-catenin protein to levels similar to FSS treatment (Figure 6D). Importantly, upon miR-100 inhibition, FSS was no longer able to confer mechanosensitive control of β-catenin activity. Thus, suppression of miR-100, whether experimentally or in response to FSS, is sufficient to induce Wnt/β-catenin signaling. Moreover, FSS-mediated suppression of miR-100 is necessary for mechanosensitive control of β-catenin activity in osteocytes.

4 | DISCUSSION

We identified a new miR-dependent mechanism that integrates the mechanosensitive function of TGFβ and Wnt signaling pathways. The coordinated activity of these pathways is essential in many tissues, during development, in homeostasis, and disease, including in the osteoanabolic response of bone to mechanical loading. Specifically, we identified miR-100 as a crucial regulator of mechanotransduction in osteocytes. Using tibial compression (in vivo) and fluid shear stress (in vitro) models of loading, we demonstrated that miR-100 is a mechanosensitive miRNA that is downregulated in osteocytes in response to load. TGFβ signaling that is activated with fluid shear stress,[27] suppresses miR-100 expression in osteocytes and this repression is indeed essential

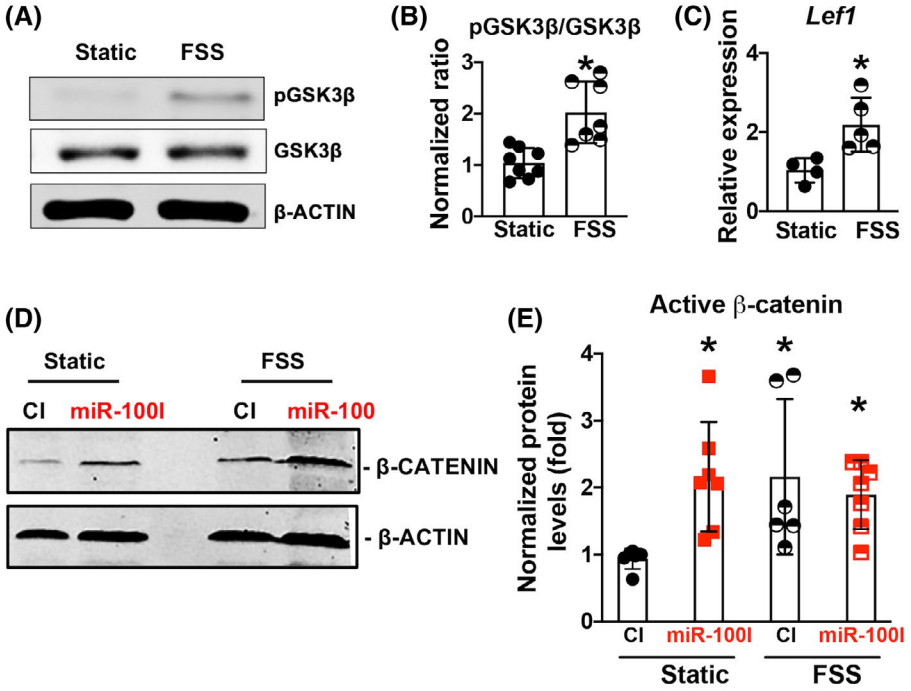

FIGURE 6 Suppression of miR-100 increases activation of Wnt/β-catenin signaling in osteocytes during fluid shear stress. Wnt/β-catenin signaling is induced in OCY454 cells subjected to 60 min of 10 dynes/cm^2 fluid shear stress (FSS) relative to cells grown in static conditions, as is evident from the increased pGSK3β/GSK3β ratio (A and B) (n = 7–8 replicates/group, mean ± SD) and the increased expression of the Wnt/β-catenin target gene, *Lef1* (C) (n = 4–5 replicates/group, mean ± SD, *$p < .05$ different from static group, unpaired t-test). Relative to CI-transfected cells, miR-100I transfected OCY454 cells have higher levels of active β-catenin in static conditions or when subjected to FSS for 1 h, which indicates that miR-100 induces Wnt/β-catenin pathway to a saturating degree that is with FSS (as observed in CI transfected cells) (D and E). Active β-catenin levels are normalized to β-actin from western blot analysis (n = 4–5 replicates/group, mean ± SD), *$p < .05$ different from the CI transfected static group, One-way ANOVA followed by Holm-Šídák's post hoc test

for induction of canonical Wnt/β-catenin pathway. Our study is unique in that we revealed a new mechanism by which TGFβ indirectly activates canonical Wnt/β-catenin in osteocytes during fluid shear stress via regulation of miR-100.

Osteocyte mechanotransduction is an intricate multifaceted process, that modulates several signaling cascades including those activated by Wnt/β-catenin, RANKL/OPG, Notch, BMP, TGFβ, PTH, and IGF1.[10,14,80] Because miRNAs can control the expression of several genes working in one or multiple pathways, it is likely that miRNAs orchestrate changes in osteocytes during mechanotransduction. By targeting multiple pathways simultaneously, miRNAs generate a unified biological response in cells. Increasingly, miRNAs have been implicated in the mechanosensitive response of bone cells, however most of these studies examine the effect of tensile or compressive stress on miRNA expression in MC3T3E1.4 osteoblasts or MLO-Y4 osteocytes.[40,42,81] Although osteocytes experience a myriad of mechanical stimuli in the form of strain, stress, shear, osmotic pressure, and fluid flow due to their unique location in the mineralized bone matrix, fluid shear stress has been identified as the primary stimulus felt by osteocytes upon load.[10,82,83] Yet, few studies have profiled fluid shear stress driven changes in the osteocyte miR transcriptome. Our study is first to generate an unbiased profile of mechanosensitive miRs in osteocytes subjected to fluid shear stress. Using the small RNA-seq approach, a total of 61 DE FSS sensitive miRs (i.e., 32 up-regulated and 29 down-regulated miRNAs) were identified in osteocytes. Among these miRNAs, many were found to be involved in osteogenic differentiation, including several with regulatory functions in cell proliferation, growth factor expression, and extracellular proteolysis, such as miR-103, miR-29b, miR-20a, miR-100, miR-148a, miR-17~92, miR-199b, miR-199a, miR-130a, miR-191 and miR-210.[38,39,84,85]

MiRNA-100 belongs to miR-99 family consisting of 3 miRNAs that are located in distinct chromosomal regions in the human and mouse genome. The three mature miRNAs of the miR-99 family, miR-99a, -99b, and -100, possess high conservation of sequence and genomic organization in mouse, rat, and human and their seed bases (ie nucleotides in positions 2–8) that are important for target recognition and binding, are identical.[78] miR-100 is encoded by a tricistronic transcript from chromosome 11 as a cluster of miR-100, Let-7a-2, and miR-125b-1 miRNAs. Although miR-99 family members may have overlapping targets, each of these miRs is DE depending on

the cellular lineage, suggesting distinct transcriptional or post-transcriptional regulation.[58,59] This is particularly apparent in the osteoclasts, where despite observing abundant expression of both miR-100 and miR-99b in osteoclast precursors, during in differentiation expression of miR-100 is induced and miR-99b is repressed.[59,86] In osteogenic cells, miR-100 inhibits BMP-induced osteoblastogenesis by suppressing expression of Runx2, as well as osteocalcin and bone-sialoprotein.[58] miR-100 is among one of the few microRNAs that has been linked to clinical osteoporosis. Expression of miR-100 is strongly correlated with BMD, and a recent study showed an longitudinal increment in miR-100 levels in the femoral bone RNA of patients with osteopenia and osteoporosis, compared to the non-osteoporotic patient samples.[60] As a freely circulating miRNA, expression levels of miR-100 are elevated in serum of patients with osteoporotic facture, which again underscores its potential as a diagnostic biomarker for osteoporosis and bone health.[60,61] Aberrant miR-100 expression has also been observed in non-traumatic osteonecrosis and osteoarthritis.[63,64] In all three skeletal etiologies, the mechanical properties of bone are compromised.[87–89] Given the strong association of miR-100 with these diseases, delineating miR-100's role in bone mass and bone quality can provide valuable insights into molecular pathways participating in these etiologies.

Although miR-100 is not the miRNA with the strongest deregulation after FSS, its abundance in osteocytes and its biological relevance in bone pathology makes this miR an important candidate for further investigation. In osteocytes, we found a stark downregulation of miR-100 levels with FSS. Inhibition of miR-100 induces the Wnt/b-catenin pathway as much as FSS alone. This ability of miR-100 to suppress Wnt signaling is potentiated by its direct binding to the 3′ UTR of Frizzled receptors to reduce their mRNA and protein levels. Apart from osteocytes, mechano-regulation of miR-100 expression has also been reported in vascular endothelial cell and human periodontal ligament stem cells,[33,65,90] where miR-100 negatively regulates mTOR, a key modulator of cell proliferation. Repression of mTOR by miR-100 has been observed in human mesenchymal cells as well. Given the conservation of miR-100 mechanosensitivity across cell types, it is possible that miR-100 also targets mTOR in osteocytes, and consequently may a key regulator of the PI3K/Akt/mTOR pathway induced by fluid shear stress.[18]

Our investigation of miR-100 function in TGFβ and Wnt signaling was guided by in-silico analysis that identified components of both pathways as miR-100 targets. In addition, in hematopoietic stem cells, the miR-100 tricistron serves as a molecular switch that balances TGFβ and Wnt signaling to promote megakaryocyte proliferation and differentiation.[78] Our studies of miR-100 in osteocytes showed that TGFβ inhibits miR-100 transcription, possibly through Smad2/3 binding sites near the miR-100 transcription start site (TSS). Other transcription factors likely cooperate with Smads to confer TGFβ-inducible regulation of miR-100 transcription. These include Hoxa10 and GATA6, both of which bind near the miR-100 TSS, and cooperate with Smad2/3 to regulate transcription in a cell type dependent manner[78,91–94]

Several studies have shown activation of Wnt/β-catenin pathway by TGFβ signaling.[95–97] In human bone marrow stromal cells, TGFβ upregulates expression of Wnt ligands and co-receptors, increasing nuclear translocation and accumulation of active β-catenin.[97] In fibroblasts, TGFβ promotes canonical Wnt signaling through repression of Axin2, a protein that forms part of the 'destruction complex' that phosphorylates and routes β-catenin toward degradation. Apart from Axin2, TGFβ represses the expression of Dkk-1 and Dkk-2, negative regulators of Wnt signaling.[95] In osteocytes, we are first to report that TGFβ acts as a positive regulator of the Wnt pathway. Here, we found that TGFβ-inducible activation of Wnt/β-catenin is achieved through repression of miR-100, which decreases the expression of important Wnt receptors. These findings offer a mechanistic explanation for the ability of FSS to coordinately induce both TGFβ and Wnt signaling, through suppression of miR-100 expression. While we have identified miR-100 as one of mechanisms by which these pathways synergize and support osteocyte mechanotransduction, based on findings reported here and by others, it is likely that Axin2 and Dkk1 also contribute to TGFβ and Wnt crosstalk.

Both TGFβ and Wnt signaling have established roles in bone development, homeostasis, and mechanoregulation.[8,26,28,98–100] At the tissue level, we showed that intact TGFβ signaling is required for the anabolic response of bone to mechanical loading.[45] Expression of a dominant negative TGFβ type II receptor under control of the osteocalcin promoter was sufficient to prevent the mechanosensitive repression of sclerostin (Sost), an inhibitor of canonical Wnt signaling that is required for bone anabolism.[45] At the cellular level, we have recently shown that osteocytes respond to fluid shear stress with a rapid and robust induction in TGFβ signaling.[27] Here we further dissect the mechanisms required for the cooperative function of TGFβ and Wnt signaling pathways by focusing on mechanosensitive control of miR-100.

Importantly, these signaling events, as well as miR function, are complex and dynamic. Both TGFβ and Wnt pathways utilize multiple canonical and non-canonical effectors and activate negative feedback loops that oppose each pathway. Future studies will be needed to better understand how these in vitro mechanisms relate temporally in vivo during the anabolic response of bone to mechanical loading. Future

analyses will benefit from the unbiased profile, captured here, of mechanoresponsive miRs in osteocytes in response to fluid shear stress. In conclusion, we identify the function of a mechanosensitive miR, miR-100, in coordinating the activity of TGFβ and Wnt signaling, two pathways with essential roles in osteocyte mechanotransduction and in the anabolic response of bone to mechanical load.

ACKNOWLEDGMENTS

The authors gratefully acknowledge R. Blelloch, our colleague in the Eli and Edythe Broad Center of Regeneration Medicine and Stem Cell Research Center UCSF, for his expert advice and helpful conversations throughout the development of this project. This research was supported by NIH-NIAMS grant R21 AR067439 (TA), NIH-NIDCR grant R01 DE019284 (TA) including a supplement from the Office of Research on Women's Health, NSF grant 1636331 (TA), Department of Defense (DoD) grant, PRORP OR130191 (TA) NIH-NIAMS grant P30 AR066262-01 (TA), the Read Research Foundation (TA).

DISCLOSURES

The authors declare no conflict of interest.

AUTHOR CONTRIBUTIONS

Study design: Neha S. Dole and Tamara Alliston; Execution of the study and data collection: Neha S. Dole, Jihee Yoon, David A. Monteiro, Jason Yang, Courtney M. Mazur, Cassandra D. Belair, and Serra Kaya; Data analysis: All authors; Data interpretation: Neha S. Dole and Tamara Alliston; Writing – original draft, Neha S. Dole; Revising manuscript and approving final version of manuscript: All authors; Supervision: Neha S. Dole and Tamara Alliston; Project leadership: Neha S. Dole and Tamara Alliston; Funding acquisition: Tamara Alliston. All authors take responsibility for the integrity of the data analysis.

ORCID

Neha S. Dole https://orcid.org/0000-0003-4675-2649

REFERENCES

1. Vining KH, Mooney DJ. Mechanical forces direct stem cell behaviour in development and regeneration. *Nat Rev Mol Cell Biol*. 2017;18(12):728-742.
2. Heisenberg C-P, Bellaïche Y. Forces in tissue morphogenesis and patterning. *Cell*. 2013;153(5):948-962.
3. Lu T-W, Chang C-F. Biomechanics of human movement and its clinical applications. *Kaohsiung J Med Sci*. 2012;28(suppl 2):S13-S25.
4. Lynch ME, Fischbach C. Biomechanical forces in the skeleton and their relevance to bone metastasis: biology and engineering considerations. *Adv Drug Deliv Rev*. 2014;79-80:119-134.
5. Chen JC, Jacobs CR. Mechanically induced osteogenic lineage commitment of stem cells. *Stem Cell Res Ther*. 2013;4(5):107.
6. Battaglino RA, Lazzari AA, Garshick E, Morse LR. Spinal cord injury-induced osteoporosis: pathogenesis and emerging therapies. *Curr Osteoporos Rep*. 2012;10(4):278-285.
7. Hall BK, Herring SW. Paralysis and growth of the musculoskeletal system in the embryonic chick. *J Morphol*. 1990;206(1):45-56.
8. Robling AG, Turner CH. Mechanical signaling for bone modeling and remodeling. *Crit Rev Eukaryot Gene Expr*. 2009;19(4):319-338.
9. Hart NH, Nimphius S, Rantalainen T, Ireland A, Siafarikas A, Newton RU. Mechanical basis of bone strength: influence of bone material, bone structure and muscle action. *J Musculoskelet Neuronal Interact*. 2017;17(3):114-139.
10. Qin L, Liu W, Cao H, Xiao G. Molecular mechanosensors in osteocytes. *Bone Res*. 2020;8:23.
11. Ciani C, Doty SB, Fritton SP. Mapping bone interstitial fluid movement: displacement of ferritin tracer during histological processing. *Bone*. 2005;37(3):379-387.
12. Fritton SP, Weinbaum S. Fluid and solute transport in bone: flow-induced mechanotransduction. *Annu Rev Fluid Mech*. 2009;41:347-374.
13. Yavropoulou MP, Yovos JG. The molecular basis of bone mechanotransduction. *J Musculoskelet Neuronal Interact*. 2016;16(3):221-236.
14. Alfieri R, Vassalli M, Viti F. Flow-induced mechanotransduction in skeletal cells. *Biophys Rev*. 2019;11(5):729-743.
15. Liu D, Genetos DC, Shao Y, et al. Activation of extracellular-signal regulated kinase (ERK1/2) by fluid shear is Ca2+- and ATP-dependent in MC3T3-E1 osteoblasts. *Bone*. 2008;42(4):644-652.
16. Choudhary S, Wadhwa S, Raisz LG, Alander C, Pilbeam CC. Extracellular calcium is a potent inducer of cyclo-oxygenase-2 in murine osteoblasts through an ERK signaling pathway. *J Bone Miner Res*. 2003;18(10):1813-1824.
17. Alford AI, Jacobs CR, Donahue HJ. Oscillating fluid flow regulates gap junction communication in osteocytic MLO-Y4 cells by an ERK1/2 MAP kinase-dependent mechanism. *Bone*. 2003;33(1):64-70.
18. Lee D-Y, Li Y-SJ, Chang S-F, et al. Oscillatory flow-induced proliferation of osteoblast-like cells is mediated by alphavbeta3 and beta1 integrins through synergistic interactions of focal adhesion kinase and Shc with phosphatidylinositol 3-kinase and the Akt/mTOR/p70S6K pathway. *J Biol Chem*. 2010;285(1):30-42.
19. Zhang B, Hou R, Zou Z, et al. Mechanically induced autophagy is associated with ATP metabolism and cellular viability in osteocytes in vitro. *Redox Biol*. 2018;14:492-498.
20. Bacabac RG, Smit TH, Mullender MG, Dijcks SJ, Van Loon JJWA, Klein-Nulend J. Nitric oxide production by bone cells is fluid shear stress rate dependent. *Biochem Biophys Res Commun*. 2004;315(4):823-829.
21. Kunnen SJ, Leonhard WN, Semeins C, et al. Fluid shear stress-induced TGF-β/ALK5 signaling in renal epithelial cells is modulated by MEK1/2. *Cell Mol Life Sci*. 2017;74(12):2283-2298.
22. Sheng X, Sheng Y, Liu Y, Li X, Shu B, Li D. Effects of FSS on the expression and localization of the core proteins in two Wnt signaling pathways, and their association with ciliogenesis. *Int J Mol Med*. 2018;42(4):1809-1818.
23. Kouzbari K, Hossan MR, Arrizabalaga JH, et al. Oscillatory shear potentiates latent TGF-β1 activation more than steady shear as demonstrated by a novel force generator. *Sci Rep*. 2019;9(1):6065.

24. Rubin J, Rubin C, Jacobs CR. Molecular pathways mediating mechanical signaling in bone. *Gene*. 2006;367:1-16.
25. Rangaswami H, Schwappacher R, Tran T, et al. Protein kinase G and focal adhesion kinase converge on Src/Akt/β-catenin signaling module in osteoblast mechanotransduction. *J Biol Chem*. 2012;287(25):21509-21519.
26. Lara-Castillo N, Kim-Weroha NA, Kamel MA, et al. In vivo mechanical loading rapidly activates β-catenin signaling in osteocytes through a prostaglandin mediated mechanism. *Bone*. 2015;76:58-66.
27. Monteiro DA, Dole NS, Campos JL, et al. Fluid shear stress generates a unique signaling response by activating multiple TGFβ family type I receptors in osteocytes. *FASEB J*. 2021;35(3):e21263.
28. Spatz JM, Wein MN, Gooi JH, et al. The Wnt inhibitor sclerostin is up-regulated by mechanical unloading in osteocytes in vitro. *J Biol Chem*. 2015;290(27):16744-16758.
29. Friedman RC, Farh KK-H, Burge CB, Bartel DP. Most mammalian mRNAs are conserved targets of microRNAs. *Genome Res*. 2009;19(1):92-105.
30. Bartel DP. MicroRNAs: target recognition and regulatory functions. *Cell*. 2009;136(2):215-233.
31. Bartel DP. Metazoan microRNAs. *Cell*. 2018;173(1):20-51.
32. Neth P, Nazari-Jahantigh M, Schober A, Weber C. MicroRNAs in flow-dependent vascular remodelling. *Cardiovasc Res*. 2013;99(2):294-303.
33. Kumar S, Kim CW, Simmons RD, Jo H. Role of flow-sensitive microRNAs in endothelial dysfunction and atherosclerosis. *Arterioscler Thromb Vasc Biol*. 2014;34(10):2206-2216.
34. Rysä J, Tokola H, Ruskoaho H. Mechanical stretch induced transcriptomic profiles in cardiac myocytes. *Sci Rep*. 2018;8(1):4733.
35. Arfat Y, Xiao W-Z, Ahmad M, et al. Role of microRNAs in osteoblasts differentiation and bone disorders. *Curr Med Chem*. 2015;22(6):748-758.
36. Hu R, Li H, Liu W, Yang L, Tan Y-F, Luo X-H. Targeting miRNAs in osteoblast differentiation and bone formation. *Expert Opin Ther Targets*. 2010;14(10):1109-1120.
37. Lozano C, Duroux-Richard I, Firat H, Schordan E, Apparailly F. MicroRNAs: key regulators to understand osteoclast differentiation? *Front Immunol*. 2019;10:375.
38. Lian JB, Stein GS, van Wijnen AJ, et al. MicroRNA control of bone formation and homeostasis. *Nat Rev Endocrinol*. 2012;8(4):212-227.
39. van Wijnen AJ, van de Peppel J, van Leeuwen JP, et al. MicroRNA functions in osteogenesis and dysfunctions in osteoporosis. *Curr Osteoporos Rep*. 2013;11(2):72-82.
40. Mai Z, Peng Z, Zhang J, et al. miRNA expression profile during fluid shear stress-induced osteogenic differentiation in MC3T3-E1 cells. *Chin Med J*. 2013;126(8):1544-1550.
41. Chen Z, Zhang Y, Liang C, Chen L, Zhang G, Qian A. Mechanosensitive miRNAs and bone formation. *Int J Mol Sci*. 2017;18(8):1684.
42. Wang H, Sun Z, Wang Y, et al. miR-33-5p, a novel mechanosensitive microRNA promotes osteoblast differentiation by targeting Hmga2. *Sci Rep*. 2016;6:23170.
43. Bonewald LF. Establishment and characterization of an osteocyte-like cell line, MLO-Y4. *J Bone Miner Metab*. 1999;17(1):61-65.
44. Govey PM, Jacobs JM, Tilton SC, et al. Integrative transcriptomic and proteomic analysis of osteocytic cells exposed to fluid flow reveals novel mechano-sensitive signaling pathways. *J Biomech*. 2014;47(8):1838-1845.
45. Nguyen J, Tang SY, Nguyen D, Alliston T. Load regulates bone formation and sclerostin expression through a TGFβ-dependent mechanism. *PLoS ONE*. 2013;8(1):e53813.
46. Sugiyama T, Price JS, Lanyon LE. Functional adaptation to mechanical loading in both cortical and cancellous bone is controlled locally and is confined to the loaded bones. *Bone*. 2010;46(2):314-321.
47. Dole NS, Mazur CM, Acevedo C, et al. Osteocyte-intrinsic TGF-β signaling regulates bone quality through perilacunar/canalicular remodeling. *Cell Rep*. 2017;21(9):2585-2596.
48. Kelly NH, Schimenti JC, Ross FP, van der Meulen MCH. Transcriptional profiling of cortical versus cancellous bone from mechanically-loaded murine tibiae reveals differential gene expression. *Bone*. 2016;86:22-29.
49. Dole NS, Kapinas K, Kessler CB, et al. A single nucleotide polymorphism in osteonectin 3′ untranslated region regulates bone volume and is targeted by miR-433. *J Bone Miner Res*. 2015;30(4):723-732.
50. Smith SS, Dole NS, Franceschetti T, Hrdlicka HC, Delany AM. MicroRNA-433 dampens glucocorticoid receptor signaling, impacting circadian rhythm and osteoblastic gene expression. *J Biol Chem*. 2016;291(41):21717-21728.
51. Belair CD, Hu T, Chu B, Freimer JW, Cooperberg MR, Blelloch RH. High-throughput, efficient, and unbiased capture of small RNAs from low-input samples for sequencing. *Sci Rep*. 2019;9(1):2262.
52. Bouhaddioui W, Provost PR, Tremblay Y. Identification of most stable endogenous control genes for microRNA quantification in the developing mouse lung. *PLoS ONE*. 2014;9(11):e111855.
53. Bustin SA, Benes V, Garson JA, et al. The MIQE guidelines: minimum information for publication of quantitative real-time PCR experiments. *Clin Chem*. 2009;55(4):611-622.
54. Rao X, Huang X, Zhou Z, Lin X. An improvement of the 2ˆ(-delta delta CT) method for quantitative real-time polymerase chain reaction data analysis. *Biostat Bioinforma Biomath*. 2013;3(3):71-85.
55. Veeman MT, Slusarski DC, Kaykas A, Louie SH, Moon RT. Zebrafish prickle, a modulator of noncanonical Wnt/Fz signaling, regulates gastrulation movements. *Curr Biol*. 2003;13(8):680-685.
56. Lu T-P, Lee C-Y, Tsai M-H, et al. miRSystem: an integrated system for characterizing enriched functions and pathways of microRNA targets. *PLoS ONE*. 2012;7(8):e42390.
57. Catalanotto C, Cogoni C, Zardo G. MicroRNA in control of gene expression: an overview of nuclear functions. *Int J Mol Sci*. 2016;17(10):1712.
58. Zeng Y, Qu X, Li H, et al. MicroRNA-100 regulates osteogenic differentiation of human adipose-derived mesenchymal stem cells by targeting BMPR2. *FEBS Lett*. 2012;586(16):2375-2381.
59. Zhou L, Song H-Y, Gao L-L, Yang L-Y, Mu S, Fu Q. MicroRNA-100-5p inhibits osteoclastogenesis and bone resorption by regulating fibroblast growth factor 21. *Int J Mol Med*. 2019;43(2):727-738.
60. Kelch S, Balmayor ER, Seeliger C, Vester H, Kirschke JS, van Griensven M. miRNAs in bone tissue correlate to bone mineral density and circulating miRNAs are gender independent in osteoporotic patients. *Sci Rep*. 2017;7(1):15861.

61. Seeliger C, Karpinski K, Haug AT, et al. Five freely circulating miRNAs and bone tissue miRNAs are associated with osteoporotic fractures. *J Bone Miner Res*. 2014;29(8):1718-1728.
62. Hou Q, Huang Y, Luo Y, et al. MiR-351 negatively regulates osteoblast differentiation of MSCs induced by (+)-cholesten-3-one through targeting VDR. *Am J Transl Res*. 2017;9(11):4963-4973.
63. Wei B, Wei W, Wang L, Zhao B. Differentially expressed microRNAs in conservatively treated nontraumatic osteonecrosis compared with healthy controls. *Biomed Res Int*. 2018;2018:9015758.
64. Wu J, Kuang L, Chen C, et al. miR-100-5p-abundant exosomes derived from infrapatellar fat pad MSCs protect articular cartilage and ameliorate gait abnormalities via inhibition of mTOR in osteoarthritis. *Biomaterials*. 2019;206:87-100.
65. Frith JE, Kusuma GD, Carthew J, et al. Mechanically-sensitive miRNAs bias human mesenchymal stem cell fate via mTOR signalling. *Nat Commun*. 2018;9(1):257.
66. Tian L, Zheng F, Li Z, et al. miR-148a-3p regulates adipocyte and osteoblast differentiation by targeting lysine-specific demethylase 6b. *Gene*. 2017;627:32-39.
67. Patel V, Carrion K, Hollands A, et al. The stretch responsive microRNA miR-148a-3p is a novel repressor of IKBKB, NF-κB signaling, and inflammatory gene expression in human aortic valve cells. *FASEB J*. 2015;29(5): 1859-1868.
68. Pan B-L, Tong Z-W, Li S-D, et al. Decreased microRNA-182-5p helps alendronate promote osteoblast proliferation and differentiation in osteoporosis via the Rap1/MAPK pathway. *Biosci Rep*. 2018;38(6):BSR20180696.
69. Chen X, Gu S, Chen B-F, et al. Nanoparticle delivery of stable miR-199a-5p agomir improves the osteogenesis of human mesenchymal stem cells via the HIF1a pathway. *Biomaterials*. 2015;53:239-250.
70. Heuslein JL, Gorick CM, McDonnell SP, Song J, Annex BH, Price RJ. Exposure of endothelium to biomimetic flow waveforms yields identification of miR-199a-5p as a potent regulator of arteriogenesis. *Mol Ther - Nucleic Acids*. 2018;12:829-844.
71. Fu Y, Xu Y, Chen S, Ouyang Y, Sun G. MiR-151a-3p promotes postmenopausal osteoporosis by targeting SOCS5 and activating JAK2/STAT3 signaling. *Rejuvenation Res*. 2020;23(4):313-323.
72. Takahara S, Lee SY, Iwakura T, et al. Altered expression of microRNA during fracture healing in diabetic rats. *Bone Joint Res*. 2018;7(2):139-147.
73. Weilner S, Skalicky S, Salzer B, et al. Differentially circulating miRNAs after recent osteoporotic fractures can influence osteogenic differentiation. *Bone*. 2015;79:43-51.
74. Yu T, You X, Zhou H, et al. MiR-16-5p regulates postmenopausal osteoporosis by directly targeting VEGFA. *Aging*. 2020;12(10):9500-9514.
75. KrishnaPriya S, Banerjee S, Karunagaran D, Suraishkumar GK. Non-coding RNAs in fluid shear stress-driven and reactive oxygen species-mediated colon cancer metastasis. *bioRxiv*. 2020:2020.08.31.275065.
76. Ni C-W, Qiu H, Jo H. MicroRNA-663 upregulated by oscillatory shear stress plays a role in inflammatory response of endothelial cells. *Am J Physiol Heart Circ Physiol*. 2011;300(5): H1762-H1769.
77. Mao G, Zhang Z, Huang Z, et al. MicroRNA-92a-3p regulates the expression of cartilage-specific genes by directly targeting histone deacetylase 2 in chondrogenesis and degradation. *Osteoarthr Cartil*. 2017;25(4):521-532.
78. Emmrich S, Rasche M, Schöning J, et al. miR-99a/100~125b tricistrons regulate hematopoietic stem and progenitor cell homeostasis by shifting the balance between TGFβ and Wnt signaling. *Genes Dev*. 2014;28(8):858-874.
79. Jiang Q, He M, Guan S, et al. MicroRNA-100 suppresses the migration and invasion of breast cancer cells by targeting FZD-8 and inhibiting Wnt/β-catenin signaling pathway. *Tumor Biol*. 2016;37(4):5001-5011.
80. Chen W, Qing H, He Y, Wang J, Zhu Z, Wang H. Gene expression patterns of osteocyte-like MLO-Y4 cells in response to cyclic compressive force stimulation. *Cell Biol Int*. 2010;34(5):425-432.
81. Chen Z, Zhao F, Qi Y, et al. Simulated microgravity alters the expression of cytoskeleton- and ATP-binding-related genes in MLO-Y4 osteocytes. *Acta Astronaut*. 2016;129:186-192.
82. Wittkowske C, Reilly GC, Lacroix D, Perrault CM. In vitro bone cell models: impact of fluid shear stress on bone formation. *Front Bioeng Biotechnol*. 2016;4:87.
83. Uda Y, Azab E, Sun N, Shi C, Pajevic PD. Osteocyte mechanobiology. *Curr Osteoporos Rep*. 2017;15(4):318-325.
84. Kapinas K, Delany AM. MicroRNA biogenesis and regulation of bone remodeling. *Arthritis Res Ther*. 2011;13(3):220.
85. Garcia J, Delany AM. MicroRNAs regulating TGFβ and BMP signaling in the osteoblast lineage. *Bone*. 2021;143:115791.
86. Franceschetti T, Dole NS, Kessler CB, Lee S-K, Delany AM. Pathway analysis of microRNA expression profile during murine osteoclastogenesis. *PLoS ONE*. 2014;9(9):e107262.
87. Zimmermann EA, Schaible E, Gludovatz B, et al. Intrinsic mechanical behavior of femoral cortical bone in young, osteoporotic and bisphosphonate-treated individuals in low- and high energy fracture conditions. *Sci Rep*. 2016;6(1):21072.
88. Ma J-X, He W-W, Zhao J, et al. Bone microarchitecture and biomechanics of the necrotic femoral head. *Sci Rep*. 2017;7(1):13345.
89. Peters AE, Akhtar R, Comerford EJ, Bates KT. The effect of ageing and osteoarthritis on the mechanical properties of cartilage and bone in the human knee joint. *Sci Rep*. 2018;8(1):5931.
90. Pankratz F, Hohnloser C, Bemtgen X, et al. MicroRNA-100 suppresses chronic vascular inflammation by stimulation of endothelial autophagy. *Circ Res*. 2018;122(3):417-432.
91. Lu Y, Zhao X, Liu QI, et al. lncRNA MIR100HG-derived miR-100 and miR-125b mediate cetuximab resistance via Wnt/β-catenin signaling. *Nat Med*. 2017;23(11):1331-1341.
92. Chia CY, Madrigal P, Denil SLIJ, et al. GATA6 cooperates with EOMES/SMAD2/3 to deploy the gene regulatory network governing human definitive endoderm and pancreas formation. *Stem cell reports*. 2019;12(1):57-70.
93. Hill CS. Transcriptional control by the SMADs. *Cold Spring Harb Perspect Biol*. 2016;8(10):a022079.
94. Shah CA, Wang H, Bei L, Platanias LC, Eklund EA. HoxA10 regulates transcription of the gene encoding transforming growth factor beta2 (TGFbeta2) in myeloid cells. *J Biol Chem*. 2011;286(4):3161-3176.
95. Gillespie J, Ross RL, Corinaldesi C, et al. Transforming growth factor β activation primes canonical Wnt signaling through down-regulation of axin-2. *Arthritis Rheumatol*. 2018;70(6):932-942.
96. Nlandu-Khodo S, Neelisetty S, Phillips M, et al. Blocking TGF-β and β-catenin epithelial crosstalk exacerbates CKD. *J Am Soc Nephrol*. 2017;28(12):3490-3503.

97. Zhou S, Eid K, Glowacki J. Cooperation between TGF-β and Wnt pathways during chondrocyte and adipocyte differentiation of human marrow stromal cells. *J Bone Miner Res*. 2003;19(3):463-470.
98. Tang SY, Alliston T. Regulation of postnatal bone homeostasis by TGFβ. *Bonekey Rep*. 2013;2:255.
99. Kramer I, Halleux C, Keller H, et al. Osteocyte Wnt/β-catenin signaling is required for normal bone homeostasis. *Mol Cell Biol*. 2010;30(12):3071-3085.
100. Bonewald LF, Johnson ML. Osteocytes, mechanosensing and Wnt signaling. *Bone*. 2008;42(4):606-615.

SUPPORTING INFORMATION

Additional supporting information may be found in the online version of the article at the publisher's website.

How to cite this article: Dole NS, Yoon J, Monteiro DA, et al. Mechanosensitive miR-100 coordinates TGFβ and Wnt signaling in osteocytes during fluid shear stress. *FASEB J*. 2021;35:e21883. https://doi.org/10.1096/fj.202100930